Bergische Universität Wuppertal

Fachbereich Mathematik und Naturwissenschaften

Institute of Mathematical Modelling, Analysis and Computational Mathematics (IMACM)

Preprint BUW-IMACM 13/2

Sebastian Schmitz (ICS Lugano and Siemens Energy), Georg Rollmann (Siemens Energy)
Hanno Gottschalk (BUW / IMACM) and Rolf Krause (ICS Lugano)

RISK ESTIMATION FOR LCF CRACK INITIATION

February 2013

http://www.math.uni-wuppertal.de

RISK ESTIMATION FOR LCF CRACK INITIATION

Sebastian Schmitz*
Gas Turbine Department of Materials and Technology
Siemens AG Energy
Mülheim an der Ruhr, Nordrhein-Westfalen, 45473
Germany
Email: schmitz.sebastian@siemens.com

Georg Rollmann
Gas Turbine Department of Materials and Technology
Siemens AG Energy
Mülheim an der Ruhr, Nordrhein-Westfalen, 45473
Germany
Email: georg.rollmann@siemens.com

Hanno Gottschalk
Faculty of Mathematics and Natural Science
Bergische Universität Wuppertal
Wuppertal, Nordrhein-Westfalen, 42097
Germany
Email: hanno.gottschalk@uni-wuppertal.de

Rolf Krause
Institute of Computational Science
Universita della Svizzerra Italiana
Lugano, Ticino, 6900
Switzerland
Email: rolf.krause@usi.ch

An accurate risk assessment for fatigue damage is of vital importance for the design and service of today's turbomachinery components. We present an approach for quantifying the probability of crack initiation due to surface driven low-cycle fatigue (LCF). This approach is based on the theory of failure-time processes and takes inhomogeneous stress fields and size effects into account. The method has been implemented as a finite-element postprocessor which uses quadrature formulae of higher order. Results of applying this new approach to an example case of a gas-turbine compressor disk are discussed.

INTRODUCTION

Due to the necessity for a more flexible service of gas turbines, low-cycle fatigue (LCF) design has become of essential importance in today's gas turbine engineering. The end of LCF-life of an engineering component is often defined by the initiation of a crack of a certain size. LCF is mostly surface driven so that an LCF crack initiates on the component's surface. In the case of polycrystalline metal the grain structure has a great influence on the LCF failure mechanism which is of stochastic nature. This can result in a statistical scatter of a factor of 10 between the highest and lowest load cycles to crack initiation, even under lab conditions.

Standard design approaches often derive a predicted component life with respect to LCF from the average life times of the most loaded points on the component plus safety factors which account for the scatter band, size effects and uncertainties in the stress and temperature fields. However, this method can have a lack of sufficient accuracy which can result in designs that are too conservative or too optimistic, for example. In particular, the Coffin-Manson-Basquin equation and Wöhler curves play an essential role in reliability estimations regarding fatigue. Moreover, size effects have

*Address all correspondence to this author. Second affiliation: Institute of Computational Science, Universita della Svizerra Italiana, Lugano, Ticino, 6900, Switzerland, Email: sebastian.schmitz@usi.ch

a significant influence on fatigue life and are mostly considered by safety factors. For more detailed discussions of fatigue confer [1], [2], [3] and [4].

In this work we focus on LCF in conjunction with polycrystalline metals and in particular on the number of load cycles until crack initiation. We present a local and probabilistic model for LCF according to [5] and [6] which we use to estimate the risk for LCF crack initiation on a compressor disk. Here, the reaction of a component to cyclic loads is taken into account via a linear elastic finite element analysis (FEA) and via Neuber shakedown, see [7], [8] and [9], respectively.

Because LCF cracks are small in the initiation phase they will only influence stress fields on micro- and mesoscales and so it is reasonable to assume that crack formation in one region of the component's surface is not influenced by the crack forming process on another part. Thus crack formation can be considered as a problem of spatial statistics [10]. Then, [5] and [6] infer that hazard rates for crack initiation have to be integrals over some local function depending on the local stress or strain fields. Therefore, hazard rates for the component can be expressed by a surface integral over some crack formation intensity function depending on local fields. The latter can also be regarded as the density for the intensity measure of a Poisson point process (PPP) in time and space, confer [11] and [12]. In [3] the role of the PPP is also emphasized in that context.

Following [5] and [6] we model the hazard rates with a rather conservative approach by means of intensity measures of Weibull type. Note that scale-shape distributions are very common in reliability statistics, confer [13]. Furthermore, we assume that the scale variable N_{det} is of the same functional form as the usual Coffin-Manson-Basquin equation, confer [5], [1] and (6) below. This results in a Weibull distribution for the number N of cycles of first crack initiation on the component as well.

In contrast to [3] this purely phenomenological approach avoids detailed modeling at the meso scale which facilitates calibration with experiments. Both approaches have the use of Weibull distributions in common. From a materials engineering point of view the model of [5] and [6] has the significant advantage – compared to standard methods in fatigue – of bypassing the standard specimen approach and considering size effects. Besides LCF-test results with standardized specimens, different strain-controlled LCF results can be used together for the calibration of the model such as results from specimens with different geometries or under different inhomogeneous strain fields.

In order to numerically compute the Weibull distribution, quadrature formulae are employed for the corresponding integration. As locations of stress concentrations result in higher nonlinearities in the integrand we use quadrature formulae of higher orders. For this purpose we interpolate the field values according to principles of mesh and finite-element generation, confer [8], [14] and [15].

Having obtained the Weibull shape and scale parameter from calibration and from numerical integration, respectively, the corresponding distribution function yields the probability for LCF crack initiation with respect to the number N of load cycles. In the design process one can decide which number N is acceptable corresponding to the assigned risk. Another important quantity of the LCF model is the local crack initiation density. This field shows how much each region of the surface contributes to the overall expected number of crack initiations and leads to critical as well as to possibly overengineered parts of the component.

This paper combines some aspects of materials engineering, reliability statistics and FEA. In the first section we consider linear elasticity, Neuber shakedown, fatigue analysis and we present the local and probabilistic model for LCF. In Section 2 we first focus on FEA. Then, we discuss numerical integration and important functions of our presented approach. The last section shows results of applying our method to an example case of a gas-turbine compressor disk.

1 A LOCAL AND PROBABILISTIC MODEL FOR LCF

In this section we discuss results of linear isotropic elasticity, Neuber shakedown and fatigue analysis. The last subsection presents the local and probabilistic model for LCF which is introduced and motivated in [5] and [6].

1.1 Linear Isotropic Elasticity and Neuber Shakedown

In this work we consider designs made from single-phased polycrystalline metal. Usually metallic material does not consist of one single crystal but of different crystalline regions which are called grains. These grains have an order of magnitude typically in the micrometer and millimeter scale. The continuum mechanical approach assumes that the considered sizing scale is large compared to the inter-atom distances. Thus the material is considered to be smeared and all quantities are continuous. In general, single crystals have anisotropic properties. In polycrystals the orientation of the grains is randomly distributed. If the grains are sufficiently small compared to the component's size, the anisotropic effects of the grains average out and an approximately isotropic material can be assumed.

In the following, we employ the continuum mechanical approach and assume isotropic material behavior at scales significantly larger than the grain size and assume sufficiently small deformations. Thus, linear isotropic elasticity can be applied to describe the behavior of components from single-phased polycrystalline metal under external loading and plasticity can be considered by Neuber shakedown. In this section we present theoretical backgrounds and closely follow Section 2 of [5] which is based on [16] and [1]. Note that our example case of a compressor disk is subject to a homogeneous temperature field so that we do not consider thermoelasticity.

Let Ω be a domain which represents the component shape filled with a deformable medium such as polycrystalline metal which is initially at equilibrium. Moreover, let ν be the normal on the surface $\partial\Omega$ of Ω, let $\mathbf{f}$ be an external load and let $\mathbf{u}$ be the three-dimensional displacement field in Ω.

Finally, let $\partial\Omega_D, \partial\Omega_N$ be a partition of the boundary where $\partial\Omega_D$ is clamped and on $\partial\Omega_N$ a normal load $\mathbf{g}$ is imposed. Then, according to [8] the mixed boundary value problem (BVP) of linear isotropic elasticity is described by:

$$\nabla \cdot \sigma^e(\mathbf{u}) + \mathbf{f} = 0 \quad \text{in } \Omega \tag{1}$$

with $\sigma^e(\mathbf{u}) = \lambda(\nabla \cdot \mathbf{u})I + \mu(\nabla\mathbf{u} + \nabla\mathbf{u}^T)$ and with boundary conditions $\mathbf{u} = 0$ on $\partial\Omega_D$ and $\sigma^e(\mathbf{u}) \cdot \nu = \mathbf{g}$ on $\partial\Omega_N$. Here, λ and μ are the Lame coefficients. The linearized strain rate tensor $\varepsilon^e(\mathbf{u})$ is defined as $\varepsilon^e(\mathbf{u}) = \frac{1}{2}(\nabla\mathbf{u} + \nabla\mathbf{u}^T)$, i.e. $\varepsilon^e_{ij} = \frac{1}{2}\left(\frac{\partial \mathbf{u}_i}{\partial x_j} + \frac{\partial \mathbf{u}_j}{\partial x_i}\right)$ for $i, j = 1,2,3$. Numerical solutions of the BVP can be computed by an FEA, confer [16], [8] and Section 2 below.

The knowledge of the threshold between elastic and plastic deformations is very important as plastic deformations can allude to an imminent residual fracture. According to [1] this threshold is often described by so-called yield criteria. In this work we use the von Mises yield criterion which is given by

$$\sqrt{\frac{1}{6}\left[(\sigma_1 - \sigma_2)^2 + (\sigma_1 - \sigma_3)^2 + (\sigma_2 - \sigma_3)^2\right]} = k_F, \tag{2}$$

where k_F is the critical value of the criterion and $\sigma_1, \sigma_2, \sigma_3$ are the principal stresses. Here, the left-hand side is proportional to the elastic strain energy of distortion. If the criterion is applied to uniaxial tensile tests the relationship $k_F = R_p/\sqrt{3}$ is obtained, where R_p is the critical value of the only nonzero principle stress in a uniaxial tensile test. The von Mises stress is defined as

$$\sigma_v = \sqrt{\frac{1}{2}\left[(\sigma_1 - \sigma_2)^2 + (\sigma_1 - \sigma_3)^2 + (\sigma_2 - \sigma_3)^2\right]}. \tag{3}$$

Thus, the previous criterion can be written as $\sigma_v = R_p$ and be used to predict yielding of metal under any loading condition from results of uniaxial tensile tests.

In the following we introduce the Ramberg-Osgood equation, confer [17]. It can be used to locally derive strain levels from scalar comparison stresses such as the von Mises stress. These strain levels determine strain-controlled fatigue life. The Ramberg-Osgood equation establishes stress-strain curves of metals near their yield points. It is very accurate in the case of smooth elastic-plastic transitions which can be observed for metals that harden with plastic deformations, for example. If K denotes the cyclic strain hardening coefficient and n the cyclic strain hardening exponent the Ramberg-Osgood equation is given by

$$\varepsilon_v = \frac{\sigma_v}{E} + \left(\frac{\sigma_v}{K}\right)^{1/n} \tag{4}$$

with Young' modulus $E = \frac{\mu(3\lambda+2\mu)}{\lambda+\mu}$. The equation defines the comparison strain ε_v, where we also write $\varepsilon_v = RO(\sigma_v)$.

Finally, we present the method of Neuber shakedown, confer [18] and [1]. Let σ_v^e denote the von Mises stress which is obtained only from linear elastic computations and let σ_v be the von Mises stress which also considers plasticity. Here, σ_v is called elastic-plastic von Mises stress. If linear elasticity leads to stress values greater than the material yield strength, Neuber shakedown will estimate corresponding elastic-plastic stress values. An energy-conservation ansatz is the foundation of Neuber's approach. It results in a relationship between the elastic von Mises stress[1] σ_v^e and the elastic-plastic von Mises stress σ_v:

$$\frac{(K_t\,\sigma_v^e)^2}{E} = \sigma_v\,\varepsilon_v = \frac{\sigma_v^2}{E} + \sigma_v\left(\frac{\sigma_v}{K}\right)^{1/n}. \tag{5}$$

Here, the Ramberg-Osgood approach is also used. K_t is the notch factor, which is set to one if σ_v^e is obtained from the BVP (1) where notches are incorporated in the boundary definition. Given the elastic comparison stress σ_v^e, we can thus calculate the elastic-plastic von Mises stress by solving (5). Thereby, we are able to obtain ε_v from (4). Note that we also write $\sigma_v = SD^{-1}(\sigma_v^e)$.

1.2 Fatigue and the Coffin-Manson-Basquin Equation

Fatigue describes the damage or failure of material under cyclic loading, confer [1], [20] and [2]. Major examples of cases where fatigue occurs are activation and deactivation operations, e.g. of motor vehicles and of gas turbines, and oscillations in technical units. Material science analyzes the physical nature of fatigue and ways to determine the number of cycles until a material fails under cyclic loading. In this work, we will consider a compressor component of a gas turbine subject to surface driven low-cycle fatigue (LCF). For backgrounds on surface driven LCF failure mechanism with respect to polycrystalline metal we refer to [1], [2], [3] and [4].

We now consider important methods of fatigue analysis and closely follow Section 3 of [5] and [1]. In fatigue specimen testing the number of cycles until failure is determined. If the tests are strain controlled so-called $E-N$ diagrams – see Figure 1 – are created, where the relationship between the strain amplitude ε_a and number N_i of cycles until crack initiation is called Wöhler curve. Usually, the range of cycles is subdivided into low-cycle fatigue (LCF) and high-cycle fatigue (HCF). LCF loads are often strain controlled, whereas HCF loads are mainly stress controlled so that corresponding $S-N$ diagrams are analyzed.

For the purpose of analysis the strain amplitude ε_a is subdivided into an elastic and plastic part where $\varepsilon_a = \varepsilon_a^{el} + \varepsilon_a^{pl}$ holds. In the LCF range the plastic part ε_a^{pl} dominates, whereas in the HCF range the elastic part $\varepsilon_a^{\text{el}}$ plays a greater role. Introducing the parameters fatigue strength σ_f' and fatigue strength exponent b we present the so-called Basquin

[1] Confer [19] for details on Neuber shakedown in conjunction with equivalent stresses. As an alternative to this method one could also use Glinka's method, confer e.g. [9].

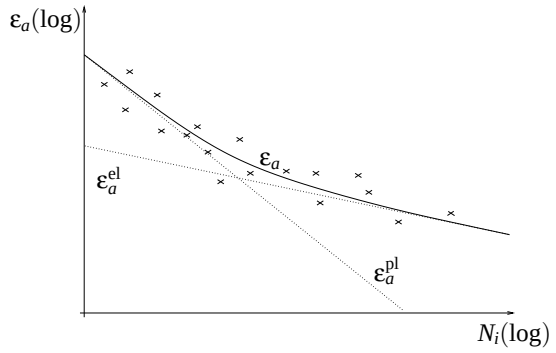

Fig. 1. EN-DIAGRAM OF A STANDARDIZED SPECIMEN.

equation $\varepsilon_a^{el} = \frac{\sigma_f'}{E}(2N_i)^b$ for the elastic part, where E is Young's modulus. Regarding the LCF range the Coffin-Manson equation $\varepsilon_a^{pl} = \varepsilon_f'(2N_i)^c$ describes the denominating plastic part, where the parameters ε_i' and c are called fatigue ductility and fatigue ductility exponent, respectively. For a detailed discussion of the physical origin of this equation we refer to [4]. The combination of the previous equations leads to the Coffin-Manson-Basquin (CMB) equation

$$\varepsilon_a = \varepsilon_a^{el} + \varepsilon_a^{pl} = \frac{\sigma_f'}{E}(2N_i)^b + \varepsilon_f'(2N_i)^c. \tag{6}$$

The parameters can be calibrated according to the test data – see Figure 1 – by means of maximum likelihood methods, for example. Confer [21], [13], [20] and Subsection 3.1 below.

Structural design concepts with respect to LCF often consider the component's surface position of highest stress and then analyze the Wöhler curve which corresponds to the conditions at that surface position. Mostly safety factors are imposed to account for the stochastic nature of fatigue, size effects[2] and for uncertainties in the stress and temperature fields. Note that sometimes several surface positions of highest stress are considered which depends on the component. This concept is called safe-life approach to fatigue design and is often used in engineering as well as very similar methods, confer [1].

Note that several extensions exist to the CMB equation (6). In particular, when approaching the HCF region, mean stress effects are of increasing importance. The modified Morrow equation is one approach that would consider such effects. For further discussions confer [2].

1.3 From Reliability Statistics to Probabilistic LCF

Now, we introduce the local and probabilistic model for LCF as presented in [5] and [6] which can be derived from reliability statistic, confer [13].

We model failure-time processes on continuous scale, although time in our context is a number of load cycles and thereby an integer number. Let N denote a continuous random variable which represents the time of crack initiation here identified with failure of a system or component. If P denotes the underlying probability measure $F_N(n) = P(N \leq n)$ is the cumulative distribution function and $f_N(n) = dF_N(n)/dn$ the density function. The survival function is defined by $S_N(n) = P(N > n) = 1 - F_N(n)$ and the hazard function by

$$h(n) = \lim_{\Delta n \to 0} \frac{P(n < N \leq n + \Delta n | N > n)}{\Delta n} = \frac{f_N(n)}{1 - F_N(n)},$$

confer [13]. h is also called hazard rate or instantaneous failure rate function. For a small step Δn the expression $h(n) \cdot \Delta n$ is an approximation for the propensity of an object or system to fail in the next time step Δn, given survival to time n. For a large number $m(n)$ of items in operation at time n the product $m(n) \cdot h(n)$ is approximately the number of failures per unit time. Defining the cumulative hazard function $H(n) = \int_0^n h(t)dt$ one can show that the survival function satisfies $S_N(n) = 1 - F_N(n) = \exp(-H(n))$. This shows that a model ansatz for the hazard function leads to a corresponding distribution function F_N.

Now, we introduce the crucial assumption for the local and probabilistic model for LCF of [5] in the case of polycrystalline metal. Consider LCF failure mechanism on the component which is represented by the domain Ω. We assume that the surface zone that is affected from the crack initiation process of a single LCF crack is small with respect to the surface of the component. This surface zone corresponds to faces of a few grains. As long range order phenomena are unusual in polycrystalline metal, we pass to the following assumption:

Assumption (L)
In any surface region $A \subseteq \partial\Omega$ the corresponding hazard rate h_A is a local functional of the elastic displacement field u in that particular region with

$$h_A(n) = \int_A \rho(n; \nabla \mathbf{u}, \nabla^2 \mathbf{u})\, dA. \tag{7}$$

Here, $\nabla \mathbf{u}$ is the Jacobian matrix and $\nabla^2 \mathbf{u}$ the Hessian of $\mathbf{u}$. Note that the loads that we consider in the given context (mainly elastic plastic stresses and strains) can all be expressed as functions of $\nabla \mathbf{u}$. The integrand ρ is called hazard density function.

Assumption (L) is also called the property of spatial additivity of hazard rates. A motivation of (L) and more detailed backgrounds can be found in [5]. For mathematical simplicity, we restrict ourselves to the case where only the dependence on elastic strains (or equivalently stresses) is taken into account.

In the case of inhomogeneous strain fields assumption (L) implies $h(n) = \int_{\partial\Omega} \rho(n; \varepsilon^e)\, dA$ for some hazard density function ρ. Because of $F_N(n) = 1 - \exp(-H(n)) = 1 - \exp\left(-\int_0^n h(t)\, dt\right)$ we obtain for the probability of failure in $\partial\Omega$ until cycle n:

$$F_N(n) = 1 - \exp\left(-\int_0^n \int_{\partial\Omega} \rho(t; \varepsilon^e)\, dA dt\right). \tag{8}$$

[2] Note that different geometries of test specimens lead to different Wöhler curves, confer [2].

The ansatz (8) can also be derived by the Poisson point process with $\rho(n;\varepsilon^e(x))$ as the intensity measure. For details on point processes we refer to [11] and [12]. The advantage of the point process is that also the probability of a given number of cracks initiations in $A \subseteq \partial\Omega$ within n load cycles can be computed via

$$P(\text{number of crack initiations on } A = q) = e^{-z}\frac{z^q}{q!} \qquad (9)$$

for $z = \int_0^n \int_A \rho(t;\varepsilon^e)\, dAdt$. But if cracks have grown sufficiently large they will mutually influence their local stress fields and thus the approach will break down.

We now establish a link to deterministic LCF analysis via CMB equation (6) which leads to an appropriate choice for the hazard density function ρ. We assume that the number N of cycles to crack initiation are Weibull distributed which can be realized by the choice of a Weibull hazard ansatz

$$\rho(n;\mathbf{x}) = \rho(n;\varepsilon^e(\mathbf{x})) = \frac{m}{N_{\det}(\varepsilon^e(\mathbf{x}))}\left(\frac{n}{N_{\det}(\varepsilon^e(\mathbf{x}))}\right)^{m-1}. \qquad (10)$$

Here, m is the Weibull shape and $N_{\det}(\varepsilon^e)$ the Weibull scale parameter which is supposed to depend on the elastic strain tensor $\varepsilon^e(\mathbf{x})$of the BVP (1). Combining (8) and (10) leads to the following model of [5]:

(Local and Probabilistic Model for LCF)
Let the scale field $N_{\det}(\mathbf{x}) = N_{\det}(\varepsilon_a(\mathbf{x}))$, $\mathbf{x} \in \partial\Omega$, be the solution of the CMB equation (6)

$$\varepsilon_a(\mathbf{x}) = \frac{\sigma_f'}{E}(2N_{\det}(\mathbf{x}))^b + \varepsilon_f'(2N_{\det}(\mathbf{x}))^c, \qquad (11)$$

where $\varepsilon_a(\mathbf{x})$ is computed from $\varepsilon^e(\mathbf{x})$ via[3] linear isotropic elasticity, from the von Mises stress $\sigma_v(\mathbf{x})$, from $\sigma_a(\mathbf{x}) = SD^{-1}(\sigma_v(\mathbf{x})/2)$ according to Neuber shakedown and from the Ramberg-Osgood equation with $\varepsilon_a(\mathbf{x}) = RO(\sigma_a(\mathbf{x}))$. Then, the local and probabilistic model for LCF is given by the cumulative distribution function

$$F_N(n) = 1 - \exp\left(-\int_0^n \int_{\partial\Omega} \frac{m}{N_{\det}}\left(\frac{s}{N_{\det}}\right)^{m-1} dAds\right). \qquad (12)$$

for $n \geq 0$ and some $m \geq 1$, which yields the probability for LCF crack initiation in the interval $[0,n]$.

The shape parameter m determines the scatter of the distribution where small values for $m \geq 1$ correspond[4] to a large scatter and where the limit $m \to \infty$ is the deterministic limit. Note that the Weibull hazard function can be easily replaced by any other differentiable hazard function with scale parameter $N_{\det}$.

The CMB parameters of the model are not the same as obtained from fitting standard specimen data. We calibrate them by means of usual maximum likelihood methods, confer Section 3, [21] and [13]. Furthermore, note that volume driven fatigue could be considered as well by replacing the surface integral in (12) with a volume integral whose integrand only differs by different material parameters. For a discussion of volume driven fatigue such as HCF confer [1].

With respect to materials engineering, the local and probabilistic model for LCF has significant advantages compared to the safe-life approach to fatigue design: The model bypasses the standard specimen approach and takes size effects into account, i.e. results from arbitrary geometries under LCF failure mechanism can be employed to calibrate our model and every position of the surface of an engineering part is considered by a surface integral which does not need information on Wöhler curves of a specific specimen. Thereby inhomogeneous stress fields are taken into account.

2 FINITE ELEMENT ANALYSIS AND POSTPROCESSING

In this section we describe our finite-element postprocessor which computes the distribution function with respect to fatigue life. First, we briefly introduce into concepts of FEA. Then, we discuss numerical integration and backgrounds on the postprocessor.

2.1 Finite Element Analysis and Lagrange Elements

In order to numerically solve the BVP (1) of linear elasticity on a three-dimensional polyhedron Ω we apply FEA, where a so-called weak formulation is considered on a finite-dimensional space of functions, confer [8], [15] and [14]. This function space and the geometry Ω are described by a mesh of finite elements, where each element consists of a three-dimensional compact and connected set T and of a finite set of basis functions $\Pi = \{\psi_1, \ldots, \psi_{n_{sh}}\}$ associated to a set of nodes $\{\mathbf{a}_1, \ldots, \mathbf{a}_{n_{sh}}\}$ in T. In the following $\{T, \Pi\}$ denotes a finite element and the functions of Π are called shape functions. The FEA solution of the BVP (1) restricted to T is then a certain linear combination of the shape functions.

Very popular finite elements are the Lagrange finite elements which are contained in most FEA packages. In our example case of a compressor disk we will use Abaqus 6.9-2 and Lagrange elements of Serendipity class (C3D20) where the shape functions are of the form

$$\psi(\mathbf{x}) = \sum_{\substack{0 \leq i_1, i_2, i_3 \leq 2 \\ i_1 + i_2 + i_3 \leq 3}} \alpha_{i_1,i_2,i_3} \cdot x_1^{i_1} x_2^{i_2} x_3^{i_3} \qquad (13)$$

for coefficients α_{i_1,i_2,i_3} determined by $\psi_i(\mathbf{a}_j) = \delta_{ij}$.

Now, principles of mesh and finite element generation are briefly introduced, where we closely follow [8].

(Mesh)
The mesh of a domain Ω is given by the union of compact and connected sets $\{T_m\}_{1 \leq m \leq N_{el}}$ with $\overline{\Omega} = \bigcup_{m=1}^{N_{el}} T_m$ and all interiors nonempty and pairwise disjoint. h_T denoting the greatest distance of two points in T we define $\mathcal{K}_h = \{T_m\}_{1 \leq m \leq N_{el}}$ where $h = \max\left\{h_T \,|\, T \in \{T_m\}_{1 \leq m \leq N_{el}}\right\}$.

[3] Confer Sections 1.1 and 1.2.
[4] $0 < m \leq 1$ is not realistic for fatigue.

The starting point for the construction of meshes is a geometric reference cell $\hat{T}$ from which the different sets are generated.

(Generated Mesh, Reference Cell)
A mesh $\mathcal{K}_h$ of a domain Ω is called generated if there exists a diffeomorphism[5] Υ_T for every $T \in \mathcal{K}_h$ and a fixed set $\hat{T}$ such that $\Upsilon_T(\hat{T}) = T$. The set $\hat{T}$ is called reference cell.

Now, we define the so-called geometric transformation which can provide the previous diffeomorphism, confer [8]:

(Geometric Transformation)
Let $\{\hat{T}, \hat{\Pi}\}$ be a finite element with shape functions $\{\hat{\psi}_1, ..., \hat{\psi}_{n_{sh}}\}$ and let $\{\mathbf{a}_1, ..., \mathbf{a}_{n_{sh}}\}$ be three-dimensional nodes. Then the geometric transformation denotes the map

$$\hat{\mathbf{x}} \longmapsto \Upsilon(\hat{\mathbf{x}}) = \sum_{i=1}^{n_{sh}} \mathbf{a}_i \hat{\psi}_i(\hat{\mathbf{x}}). \tag{14}$$

In most cases a mesh generator produces a list of n_{geo} times N_{el} nodes such as $\{\mathbf{a}_1^m, ..., \mathbf{a}_{n_{\text{geo}}}^m\}_{1 \le m \le N_{el}}$. Here, N_{el} is the number of elements again. The vectors $\{\mathbf{a}_1^m, ..., \mathbf{a}_{n_{\text{geo}}}^m\}$ are also defined as the geometric nodes of the m-th element. If Υ_m is the geometric transformation corresponding to the reference cell $\hat{T}$ and to $\{\mathbf{a}_1^m, ..., \mathbf{a}_{n_{\text{geo}}}^m\}$ with $m = 1, \ldots, N_{el}$ we set $T_m = \Upsilon_m(\hat{T})$. So we obtain m elements and can write down the following definition:

(Geometric Reference Finite Element)
If a finite element $\{\hat{T}, \hat{\Pi}_{\text{geo}}\}$ is used for mesh generation by means of given nodes

$$\{\mathbf{a}_1^m, ..., \mathbf{a}_{n_{\text{geo}}}^m\}_{1 \le m \le N_{el}}, \tag{15}$$

its geometric transformations Υ_m and setting $T_m = \Upsilon_m(\hat{T})$ for $m = 1, \ldots, N_{el}$, it is called the geometric reference finite element.

(Generation of Lagrange Elements)
Finally, we consider the generation of Lagrange elements $\{T, \Pi\}$ from a reference Lagrange element $\{\hat{T}, \hat{\Pi}\}$. Here, $\{\hat{\mathbf{a}}_i\}_{1 \le i \le n_{sh}}$ denotes the Lagrange nodes of $\{\hat{T}, \hat{\Pi}\}$ and $\{\hat{\psi}_1, ..., \hat{\psi}_{n_{sh}}\}$ the corresponding shape functions which are assigned to the nodes via $\hat{\psi}_i(\hat{\mathbf{a}}_j) = \delta_{ij}$. In this case $\hat{\Pi} = \hat{\Pi}_{\text{geo}}$ and given nodes $\{\mathbf{a}_1^m, ..., \mathbf{a}_{n_{\text{geo}}}^m\}_{1 \le m \le N_{el}}$ provide a mesh $\mathcal{K}_h$ with reference cell $\hat{T}$, geometric transformations Υ_T and sets $T = \Upsilon_T(\hat{T})$. The nodes of T satisfy $\mathbf{a}_i = \Upsilon_T(\hat{\mathbf{a}}_i)$ for $i = 1, \ldots, n_{sh}$. In order to construct Π consider for functions v the map

$$v \longmapsto \phi_T(v) = v \circ \Upsilon_T \tag{16}$$

which is linear and invertible. Then, the shape functions are given by $\Pi = \{\phi_T^{-1}(\hat{p}) \,|\, \hat{p} \in \hat{\Pi}\}$.

[5] A diffeomorphisms is continuously differentiable map whose inverse exists and is continuously differentiable as well.

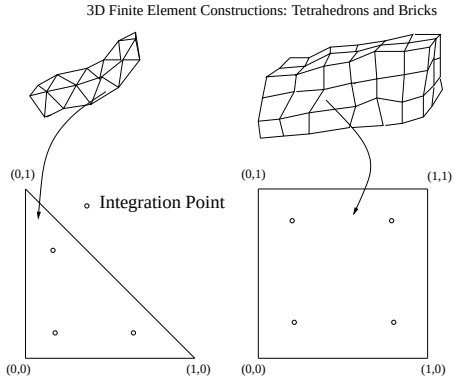

Fig. 2. GEOMETRIC TRANSFORMATION AND INTEGRATION POINTS ON THE UNIT TRIANGLE AND RECTANGLE.

2.2 Postprocessing

Recall that the local and probabilistic model for LCF is given by the cumulative distribution function (12). In the following we address numerical integration and explain how the linearized strain field $\varepsilon^e(\mathbf{x}), \mathbf{x} \in \Omega$, is computed by means of linear elastic results from FEA with Lagrange elements.

The surface integral in (12) is numerically computed by quadrature formulae. Note that we can also numerically compute volume integrals, where in (12) $\partial\Omega$ is replaced by Ω. This can be of higher interest if we extent our model to volume driven failure mechanism such as HCF. Because locations of stress concentrations will have a major contribution to our probability functional we have to consider higher nonlinearities in the integrand by our numerical approach. Therefore, we will use quadrature formulae of higher order.

Since Ω is a polyhedron which consists of finite elements we can conduct the integration of (12) on every face of a finite element which contributes to the boundary of $\partial\Omega$ and then sum up each of that integral values. Moreover, the geometric transformation (14) can be used as a chart to transform each face integration on the corresponding map area which is the unit triangle in case of tetrahedrons or the unit rectangle in case of bricks. Also see Figure 2, where exemplary geometric transformations and integration points are depicted. For more details on surface integration consider the comments to (22) below and the term of integration over submanifolds as described in [22], for example. Substitution for multiple variables is employed in case of volume integrals and thus the element integrals are transformed to the unit tetrahedron or unit brick.

(Quadrature of Order k)
Let K be an integration domain, let the l_q numbers $\omega_1, \ldots, \omega_{l_q}$ be denoted as weights and the l_q points $\xi_1, \ldots, \xi_{l_q} \in K$ as integration points (quadrature points). The weights and integration points are called quadrature of order k, if k is the

Table 1. QUADRATURE ON THE INTERVAL $K=[a,b]$ WITH $\tilde{m}=(a+b)/2$ AND $\tilde{\delta}=b-a$.

k_q	l_q	Int. Points ξ_l	Weights ω_l
1	1	$\tilde{m}$	$\tilde{\delta}$
3	2	$\tilde{m}\pm\frac{\tilde{\delta}}{2\sqrt{3}}$	$\frac{1}{2}\tilde{\delta}$
5	3	$\tilde{m}\pm\frac{\tilde{\delta}}{2}\sqrt{\frac{3}{5}}$	$\frac{5}{18}\tilde{\delta}$
		$\tilde{m}$	$\frac{8}{18}\tilde{\delta}$
7	4	$\tilde{m}\pm\frac{\tilde{\delta}}{2}\left(\sqrt{(15+2\sqrt{30})/35}\right)$	$\left(\frac{1}{4}-\frac{1}{12}\sqrt{\frac{5}{6}}\right)\tilde{\delta}$
		$\tilde{m}\pm\frac{\tilde{\delta}}{2}\left(\sqrt{(15-2\sqrt{30})/35}\right)$	$\left(\frac{1}{4}+\frac{1}{12}\sqrt{\frac{5}{6}}\right)\tilde{\delta}$

largest integer such that

$$\int_K p(\mathbf{x})dx=\sum_{l=1}^{l_q}\omega_l p(\xi_l)\quad\text{for all}$$
$$p\in\mathbf{P}_k=\left\{\sum_{\substack{0\le i_1,\dots,i_d\le k\\ i_1+\dots+i_d\le k}}\alpha_{i_1,\dots,i_d}x_1^{i_1}\dots x_d^{i_d}\;\middle|\;\alpha_{i_1,\dots,i_d}\text{ real}\right\}. \tag{17}$$

With respect to intervals $[a,b]$ Table 1 shows corresponding weights and integration points. Confer Table 8.1. and 8.2. in [8] as well, where Table 8.2 contains quadrature formulae for triangles. Note that a quadrature on an interval can be used to obtain a quadrature on a rectangle $[a,b]\times[c,d]$ by subdividing the multidimensional integral into one-dimensional integrals. This results into the four integration points of the unit rectangle in Figure 2. Similarly we obtain quadrature formulae for bricks and thus can numerically integrate over volumes of finite elements. For volume quadratures on tetrahedrons and quadratures of higher orders we again refer to Section 8 in [8].

Considering the finite element generation, we use the coordinates of the nodes, the displacements of the nodes and the connectivity (information on which nodes belong to a specific element). Moreover, we have to employ the explicit form of the shape functions $\{\hat{\psi}_0,\dots,\hat{\psi}_{n_{sh}}\}$ of the reference Lagrange element $\{\hat{T},\hat{\Pi}\}$. Then, we obtain the geometric transformation for every finite element $\{T_l,\Pi_l\}$ according to (14) and the local displacements on every T_l according to (16):

$$\hat{\mathbf{x}}\longmapsto(\mathbf{u}_{T_l}\circ\Upsilon_{T_l})(\hat{\mathbf{x}})=\sum_{k=1}^{n_{sh}}\mathbf{u}_k\hat{\psi}_k(\hat{\mathbf{x}}), \tag{18}$$

with $\mathbf{u}_k$ displacement vectors at each node of $\{T_l,\Pi_l\}$.

Now, the computation of the linearized strain rate tensor ε^e is explained. We will express the fields in dependence of $\hat{\mathbf{x}}\in\hat{T}$. Let $\mathbf{x}$ be the coordinates that describe the locations of T_l. Because of the geometric transformation we have $\mathbf{x}=\Upsilon_{T_l}(\hat{\mathbf{x}})$ for some $\hat{\mathbf{x}}\in\hat{T}$. Recall the form of the linearized strain rate tensor:

$$\varepsilon_{ij}(\mathbf{x})=\frac{1}{2}\left(\frac{\partial u_i}{\partial x_j}(\mathbf{x})+\frac{\partial u_j}{\partial x_i}(\mathbf{x})\right),\quad i,j\in\{1,2,3\},$$

with u_i components of displacement vector $\mathbf{u}$. In order to express the strain completely in coordinates $\hat{\mathbf{x}}$ of the reference element $\{\hat{T},\hat{\Pi}\}$, one has to consider the chain rule and to implement

$$\frac{\partial\left(\mathbf{u}_{T_l}\circ\Upsilon_{T_l}\right)_i}{\partial\hat{x}_j}(\hat{\mathbf{x}})=\sum_{k=1}^{n_{sh}}(\mathbf{u}_k)_i\frac{\partial\hat{\psi}_k}{\partial\hat{x}_j}(\hat{\mathbf{x}}),\quad i\in\{1,2,3\}, \tag{19}$$

(which follows from (18)) and

$$\frac{\partial\left(\Upsilon_{T_l}\right)_i}{\partial\hat{x}_j}(\hat{\mathbf{x}})=\sum_{k=1}^{n_{sh}}(\mathbf{a}_k)_i\frac{\partial\hat{\psi}_k}{\partial\hat{x}_j}(\hat{\mathbf{x}}),\quad i,j\in\{1,2,3\}. \tag{20}$$

(20) leads to the Jacobian $\nabla\Upsilon_{T_l}(\hat{x})$ of the geometric transformation Υ_{T_l} of (14).

Considering material parameters such as Young's modulus E and Poisson's ratio ν, we can now compute with respect to the coordinates $\hat{\mathbf{x}}\in\hat{T}$ the stress tensor, the von Mises stress (3), the elastic-plastic von Mises stress σ_v according to Neuber shakedown (5), the comparison strain ε_v according to the Ramberg-Osgood equation (4) and finally N_{det} according to the CMB approach (11).

Recalling (12), we explain the computation of $F_N(n)$: Let $\mathcal{F}_{ij}$ be the j-th face of the i-th element for $i=1,\dots,N_{el}$ and $j=1,\dots,N_F$, where N_F is the number of faces of the considered element type. Let $\delta_{\mathcal{F}_{ij},\partial\Omega}$ be 1 if $\mathcal{F}_{ij}$ is a subset of the surface $\partial\Omega$ with area greater than 0, otherwise let it be 0. Then,

$$\begin{aligned}&\int_0^n\int_{\partial\Omega}\frac{m}{N_{\text{det}}}\left(\frac{s}{N_{\text{det}}}\right)^{m-1}dAds=n^m\int_{\partial\Omega}\left(\frac{1}{N_{\text{det}}}\right)^m dA\\&=n^m\sum_{i=1}^{N_{el}}\sum_{j=1}^{N_F}\left[\delta_{\mathcal{F}_{ij},\partial\Omega}\cdot\int_{\mathcal{F}_i}\left(\frac{1}{N_{\text{det}}}\right)^m dA\right].\end{aligned} \tag{21}$$

In case of bricks we integrate over the unit rectangle as map area:

$$\int_{\mathcal{F}_{ij}}\left(\frac{1}{N_{\text{det}}}\right)^m dA=\int_{\square}\left(\frac{1}{N_{\text{det}}(\gamma_{ij}(\mathbf{s}))}\right)^m\sqrt{g^{\gamma_{ij}}(\mathbf{s})}ds \tag{22}$$

with charts $\gamma_{i1}(\mathbf{s})=\Upsilon_{T_i}(0,s_1,s_2),\gamma_{i2}(\mathbf{s})=\Upsilon_{T_i}(1,s_1,s_2),\gamma_{i3}(\mathbf{s})=\Upsilon_{T_i}(s_1,0,s_2),\gamma_{i4}(\mathbf{s})=\Upsilon_{T_i}(s_1,1,s_2),\gamma_{i5}(\mathbf{s})=\Upsilon_{T_i}(s_1,s_2,0),\gamma_{i6}(\mathbf{s})=\Upsilon_{T_i}(s_1,s_2,1)$ for $\mathbf{s}=(s_1,s_2)\in[0,1]\times[0,1]$ and with the Gram determinant $g^{\gamma_{ij}}(\mathbf{s})=\det\left(\nabla\gamma_{ij}(\mathbf{s})^T\nabla\gamma_{ij}(\mathbf{s})\right)$, where $\nabla\gamma_{ij}$

is the Jacobian of γ_{ij}. In case of tetrahedrons we integrate over the unit triangle Δ as map area with charts $\gamma_{i1}(\mathbf{s}) = \Upsilon_{T_i}(0,s_1,s_2), \gamma_{i2}(\mathbf{s}) = \Upsilon_{T_i}(s_1,0,s_2), \gamma_{i3}(\mathbf{s}) = \Upsilon_{T_i}(s_1,s_2,0), \gamma_{i4}(\mathbf{s}) = \Upsilon_{T_i}(s_1,s_2,1-s_1-s_2)$. In case of volume integral the Gram determinant (21) has to be replace by $|\det(D\Upsilon_{T_i})|$ and the integration is conducted over the whole reference brick and tetrahedron, respectively.

Now, we use quadrature formula $(\xi_l,\omega_l)_{l=1,\dots,l_q}$ to numerically compute the cumulative distribution function (12). Considering (21) and (22) leads to:

$$\begin{aligned} &F_N(n) \\ &\approx 1-\exp\left(-n^m \sum_{i=1}^{N_{el}} \sum_{j=1}^{N_F} \delta_{\mathcal{F}_{ij},\partial\Omega} \sum_{l=1}^{l_q} \frac{\sqrt{g^{\gamma_{ij}}(\xi_l)}}{(N_{\det}(\gamma_{ij}(\xi_l)))^m} \cdot \omega_l\right) \\ &= 1-\exp\left(-\left(\frac{n}{\eta}\right)^m\right), \end{aligned} \tag{23}$$

where we defined the scale value

$$\eta = \left(\sum_{i=1}^{N_{el}} \sum_{j=1}^{N_F} \delta_{\mathcal{F}_{ij},\partial\Omega} \sum_{l=1}^{l_q} \frac{\sqrt{g^{\gamma_{ij}}(\xi_l)}}{(N_{\det}(\gamma_{ij}(\xi_l)))^m} \cdot \omega_l\right)^{-1/m}. \tag{24}$$

In case of bricks use Table 1 and in case of tetrahedrons Table 8.2 in [8]. Equation (23) shows that the Weibull hazard ansatz in the local and probabilistic LCF model leads to a Weibull distribution for the component Ω under surface driven and strain-controlled LCF failure mechanism. Here, the scale value η is computed according to chosen finite element types and quadrature formula. As mentioned in Subsection 1.3 the parameters of the Ramberg-Osgood, the CMB equation and the shape parameter m have to be calibrated via LCF-test results.

In this work the main input for FEA postprocessing are the coordinates and displacements of the nodes and the connectivity. Moreover, values for the parameters of our model must be given which depend on the considered material. Note that we do not employ additional information of FEA packages on which faces $\mathcal{F}_{ij}$ contribute to the surface $\partial\Omega$ with a non-vanishing area, so that we identify the surface only via the main FEA output. This identification of the surface can numerically fail if finite elements are significantly distorted. But in most applications there are at most a few of such distorted elements and their contribution to the overall probability of crack initiation can often be neglected.

3 LCF-LIFE ESTIMATION FOR A COMPRESSOR DISK

In this section we consider a linear elastic Abaqus model of a compressor disk, see Figure 3, and estimate its Weibull distribution with respect to LCF life by means of our postprocessor.

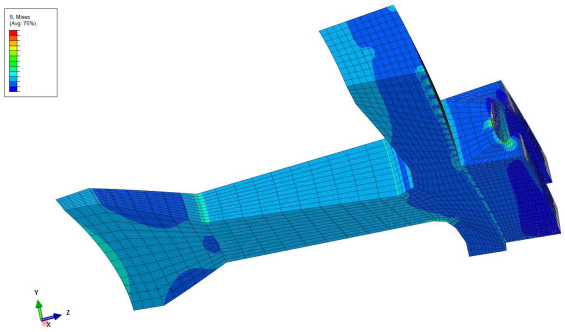

Fig. 3. FEA RESULTS OF ABAQUS 6.9-2 FOR THE VON MISES STRESS FIELD OF THE COMPRESSOR DISK.

3.1 FEA Model and Parameter Calibration

In the following we consider two states of the compressor disk: The shutdown state and the operating state. Before the gas turbine is activated the compressor disk is subjected to a homogeneous temperature field but to no stresses. This constitutes the shutdown state. In the operating state the disk is subjected to an inhomogeneous stress field. The temperature field is still homogeneous, but its value has increased. It is assumed that the fields are stationary which is only an approximation regarding the real operating state of the disk. As a conservative estimation the temperature field of the shutdown state is set equal to that one of the final state, otherwise thermal mechanical fatigue (TMF) has to be considered. The transition from the shutdown state to the operating state and then back to the shutdown state is considered as one load cycle. It is assumed that the shutdown and operating state stay the same during the cycles which is again only an approximation.

An Abaqus FEA model has been created to predict the displacement and von Mises stress field of the compressor disk in the operating state. The model consists of approximately 10.000 Lagrange elements of the Serendipity class (C3D20) which is given in (13). The compressor disk is subjected to a homogeneous temperature field in the operating state which is considered in the FEA model by corresponding values for Young's modulus and Poisson's ratio. The shutdown state is already at our disposal as the displacement and stress fields are zero and the temperature field is set equal to the homogeneous one of the operating state. Thus, the main input for our postprocessor are the coordinates of the nodes, the displacements of the nodes and the connectivity of the FEA model prediction which determine the approximation of the displacement field in the operating state and the geometry of the disk.

Finally, values for the material parameters of the LCF model must be transferred. For this purpose we first calibrate the LCF model with respect to the disk material according to standardized LCF tests. Considering the cumulative distribution function $F_N(n)$ of (23) and defining $\eta = \left(\int_{\partial\Omega} N_{\det}^{-m} dA\right)^{-1/m}$, we obtain for the corresponding density

function $f_N(n)$ the expression

$$f_N(n) = \frac{d}{dn} F_N(n) = \frac{m}{\eta}\left(\frac{n}{\eta}\right)^{m-1} \exp\left[-\left(\frac{n}{\eta}\right)^{m}\right]. \quad (25)$$

We subsume the parameters of the model in a vector θ, which includes the parameters of Ramberg-Osgood and of CMB and the Weibull shape parameter m. The experimental data set for q strain-controlled LCF tests is given by $\{n_i, \varepsilon_i, \partial\Omega_i\}_{i=1,\dots,q}$. Here, n_i is the number of cycles until crack initiation and ε_i is the strain on the gauge surface $\partial\Omega_i$. We estimate (calibrate) θ by means of maximum likelihood. The log-likelihood function is defined as

$$\begin{aligned} &\log\left(\mathcal{L}\left(\{(n_i, \varepsilon_i, \partial\Omega_i)\}_{i\in\{1,\dots,q\}}\right)[\theta]\right) \\ &= \sum_{i=1}^{q} \log(f_N(\partial\Omega_i, \varepsilon_i)(n_i)[\theta]). \end{aligned} \quad (26)$$

Let $\hat{\theta}$ denote the likelihood estimator, then $\hat{\theta}$ is given by

$$\begin{aligned} &\log\left(\mathcal{L}\left(\{(n_i, \varepsilon_i, \partial\Omega_i)\}_{i\in\{1,\dots,q\}}\right)[\hat{\theta}]\right) \\ &= \max_{\theta}\left\{\log\left(\mathcal{L}\left(\{(n_i, \varepsilon_i, \partial\Omega_i)\}_{i\in\{1,\dots,q\}}\right)[\theta]\right)\right\}. \end{aligned} \quad (27)$$

Having optimized (27) and found the estimator $\hat{\theta}$ we can now apply our postprocessor to the FEA model of the compressor disk.

3.2 Results of the Probabilistic Approach to LCF

The most important result of the numerical integration in our model is the scale parameter η of the Weibull distribution (23) which yields the probability for LCF crack initiation until cycle N. The corresponding Weibull shape parameter m is already estimated by the calibration of the previous section. The Weibull distribution is shown in Figure 4 for low numbers of cycles compared to η. Here, failure is defined by the initiation of the first LCF crack on the component and PoF denotes probability of failure and N^* multiples of η.

For $N^* = 3.231 \cdot 10^{-3}$ the PoF is $6.142 \cdot 10^{-3}$%, for example. If we consider that the compressor disk consists of 44 disk segments, where one is shown in Figure 3, the probability for the initiation of the first LCF crack on the compressors disk is 0.270%. From a design perspective one decides which PoF is acceptable and then chooses the corresponding number of allowable shutdown and service cycles. Figure 5 shows the crack initiation density at N^* on the disk's surface. This density corresponds to the local expectation value for the number of crack initiations. One can see that the crack initiation density is very much localized at the bearing flank. As we first compute the Weibull scale for every boundary face we can quantify this localization. In case of the previous value for N^*, the 21 faces with the greatest crack initiation density have a combined PoF of already $5.531 \cdot 10^{-3}$% which is more than 90% of the PoF for all boundary faces.

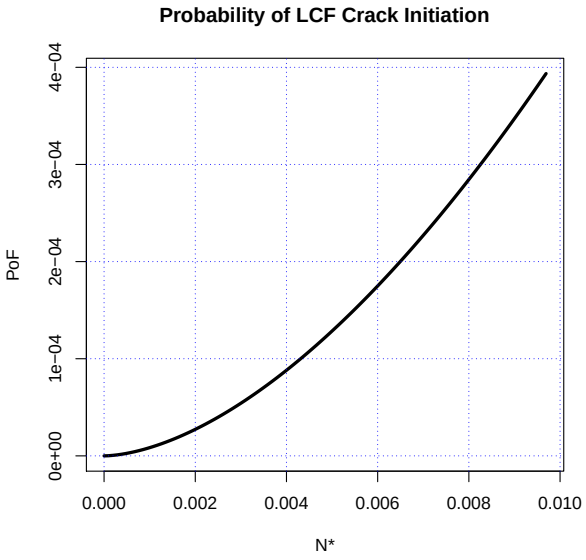

Fig. 4. WEIBULL DISTRIBUTION FOR LCF CRACK INITIATION ON THE COMPRESSOR DISK.

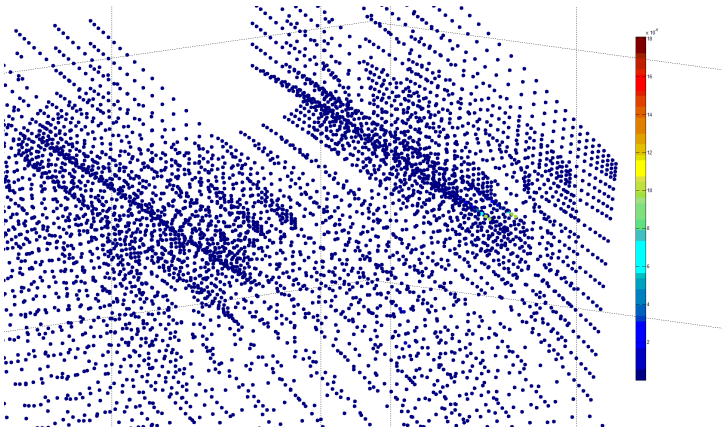

Fig. 5. CRACK INITIATION DENSITY.

With respect to field data of already operating compressor disks no failure has occurred so far. Our postprocessor predicts for that number of disks and service cycles a low PoF. Note that the assumptions for the shutdown and final state as well as the FEA model only approximate the real operating conditions of these compressor disks. In particular, consider that the field data consists of information from different gas turbines whose service conditions can be very different. Moreover, uncertainties in the model parameters θ – recall the previous section and confer the end of this section – influence the real PoF of the compressor disk. Nevertheless the model is able to predict a low PoF.

As a computational validation item of our tool we investigated whether the numerical integration converges regarding the order of the chosen quadrature. Since the FEA model consists of nonlinear Lagrange elements of Serendipity class the postprocessor employs quadratures of Table 1, confer Subsection 2.2. We computed the Weibull scale η for

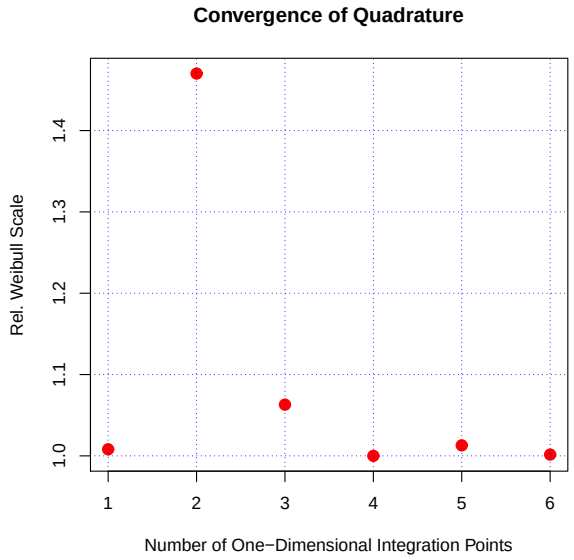

Fig. 6. CONVERGENCE OF WEIBULL SCALE REGARDING NUMBER OF INTEGRATION POINTS.

every quadrature till the order of $k = 11$, i.e. till $l_q = 6$ integration points in every dimension and thus 36 integration points on the unit rectangle. Figure 6 shows the results for each Weibull scale divided by the estimated limit and depending on the number $i = 1,\ldots,6$ of integration points in single dimension. Using 16 integration points on the unit rectangle, approximately results in a converged value for η which indicates a highly nonlinear behavior of the integrand N_{det}^{-m} of the probability function (23). This also justifies the choice of quadratures of higher order.

The cumulative distribution function $F_N(n)$ in (23) depends on the parameters θ which are calibrated as described in Subsection 3.1. Because this calibration is a statistical estimation for θ depending on LCF test data, there are uncertainties for the values of θ. This effects the real PoF but is not considered by our method so far. Taking this additional uncertainty mathematically into account can be realized by Bootstrap methods or Maximum Likelihood asymptotic theory, for example. Confer [13] for more details on these methods.

Additional to the consideration of uncertainties in the model parameters θ, the extension of our model to inhomogeneous temperature fields will be important for risk estimation for LCF crack initiation on components such as turbine blades. For this purpose a reliable temperature model for LCF is needed. Also note that the model could be extended to consider HCF, TMF and non-stationary FEA. From a design perspective there is also the interesting possibility to optimize the PoF (23) with respect to the shape Ω, i.e. find a design Ω under certain constraints such that the surface integral and PoF (23) is minimized. This is also called optimal reliability, confer [5]. Because the integrand is sufficiently regular under additional smoothness assumptions there is even a link to gradient-based shape optimization, confer [23] and [24]. This could accelerate computational optimization efforts significantly.

Acknowledgements

This work has been supported by the German federal ministry of economic affairs BMWi via an AG Turbo grant. We wish to thank the gasturbine technology department of the Siemens AG for stimulating discussions and many helpful suggestions.

References

[1] M. Bäker, H. Harders and J. Rösler, *Mechanisches Verhalten der Werkstoffe*, third edition, Vieweg+Teubner, Wiesbaden, 2008.

[2] D. Radaj and M. Vormwald, *Ermüdungsfestigkeit*, third edition, Springer, Berlin Heidelberg, 2007.

[3] B. Fedelich, A stochastic theory for the problem of multiple surface crack coalescence, International Journal of Fracture, 91, pp. 23-45, 1998.

[4] D. Sornette, T. Magnin and Y. Brechet, *The Physical Origin of the Coffin-Manson Law in Low-Cycle Fatigue*, Europhys. Lett., 20 (5), pp. 433–438, 1992.

[5] H. Gottschalk and S. Schmitz, *Optimal Reliability in Design for Fatigue Life, Part I – Existence of Optimal Shapes*, arXiv:1210.4954, 2012.

[6] S. Schmitz, T. Seibel, T. Beck, R. Rollmann, R. Krause and H. Gottschalk, *A Probabilistic Model For LCF*, in preparation

[7] P. Ciarlet, *Mathematical Elasticity - Volume I: Three-Dimensional Elasticity*, Studies in Mathematics and its Applications, Vol. 20, North-Holland, Amsterdam, 1988

[8] A. Ern and J.-L. Guermond, *Theory and Practice of Finite Elements*, Springer, New York, 2004.

[9] M. Knop, R. Jones, L. Molent, L. Wang, On Glinka and Neuber methods for calculating notch tip strains under cyclic load spectra, International Journal of Fatigue, Vol. 22, pp. 743–755, 2000.

[10] M. Sherman, Spatial Statistics and Spatio-Temporal Data: Covariance Functions and Directional Properties, Wiley Series in Probability and Statistics, 2010.

[11] A. Baddeley, P. Gregori, J. Mateu, R. Stoica and D. Stoyan, editors, *Case Studies in Spatial Point Process Modeling*, Lecture Notes in Statistics, 185, Springer, 2006.

[12] A. Klenke, *Wahrscheinlichkeitstheorie*, Springer, Berlin, 2008.

[13] L. A. Escobar and W. Q. Meeker, *Statistical Methods for Reliability Data*, Wiley-Interscience Publication, New York, 1998.

[14] P. Ciarlet, *Basic Error Estimates for Elliptic Problems*, Vol. II: Finite Element Methods, ch. 2. Handbook of Numerical Analysis, North-Holland, Amsterdam, 1991.

[15] D. Braess, *Finite Elemente - Theorie, schnelle Löser*

und Anwendungen in der Elastizitätstheorie, fourth edition, Springer, Berlin, 2007.

[16] R. B. Hetnarski and M. Reza Eslami, *Thermal Stresses - Advanced Theory and Applications*, Solid Mechanics and Its Applications, Vol. 158, Springer, Berlin, 2009.

[17] W. Ramberg and W. R. Osgood, *Description of Stress-Strain Curves by Three Parameters*, Technical Notes - National Advisory Committee For Aeronautics, No. 902, Washington DC., 1943

[18] H. Neuber, *Theory of Stress Concentration for Shear-Strained Prismatical Bodies with Arbitrary Nonlinear Stress-Strain Law*, J. Appl. Mech. 26, 544, 1961.

[19] M. Hoffmann and T. Seeger, *A Generalized Method for Estimating Elastic-Plastic Notch Stresses and Strains, Part 1: Theory*, Journal of Engineering Materials and Technology, 107, pp. 250–254, 1985.

[20] G. Schott, *Werkstoffermüdung - Ermüdungsfestigkeit*, Deutscher Verlag für Grundstoffindustrie, forth edition, Stuttgart, 1997.

[21] H.-O. Georgii, *Stochastics - Introduction to Probability and Statistics*, de Gruyter, Berlin, 2008.

[22] O. Forster, *Analysis 3*, seventh edition, Vieweg+Teubner Verlag, Wiesbaden, 2012.

[23] J. Haslinger and R. A. E. Mäkinen, *Introduction to Shape Optimization - Theory, Approximation and Computation*, SIAM - Advances in Design and Control, 2003.

[24] J. Sokolowski and J.-P. Zolesio, *Introduction to Shape Optimization - Shape Sensivity Analysis*, first edition, Springer, Berlin Heidelberg, 1992.